Functional stress responses in Glaucophyta: evidence of ethylene and ABA functions in *C. paradoxa*

Baptiste Genot[1]*, Margaret Grogan[2], Matthew Yost[3], Gabriella Iacono[1], Stephen D. Archer[1], John A Burns[1]*.

[1]Bigelow Laboratory for Ocean Sciences, East Boothbay, ME
[2]Fordham University, Bronx, NY 10458
[3]University of Maine, Orono, ME 04469
*co-corresponding authors: baptiste.genot@gmail.com, jburns@bigelow.org

Introduction

Blue-green algae belonging to the monophyletic group Glaucophyta constitute an ancient lineage that, along with Rhodophyta and Chloroplastida, is thought to have originated from a primary endosymbiosis between cyanobacteria and a phagotrophic eukaryote (Price et al., 2016). Today, 4 genera (*Cyanophora, Gloeochaete, Cyanoptyche, and Glaucocystis*) and 15 glaucophyte species are known. They are all unicellular freshwater phototrophs and are notably characterized by non-stacked thylakoids and two unique traits inherited from a prokaryotic ancestor: peptidoglycan layers around the plastid called muroplast or cyanelle in glaucophytes and carboxysome-like bodies (Jackson et al., 2015; Price et al., 2016). For these reasons, glaucophytes are sometimes called "living fossils," as they represent one of the earliest diverging lineages within the Archaeplastida and retain traits of the cyanobacterial endosymbiont that are absent in red or green algae.

Cyanophora paradoxa is the only species whose nuclear genome has entirely been sequenced (Price et al., 2016, 2012); it has therefore been used as a model glaucophyte in studies of the early evolution of photosynthetic eukaryotes. *C. paradoxa* cells are ovoid (9–16 µm) with two cilia and one to two plastids (Jackson et al., 2015). They can easily be cultivated in basic freshwater media in a light and temperature-controlled chamber, making them a good representative of glaucophyte taxa. These algae are found worldwide in habitats poor or rich in nutrients, such as lakes, swamps, acidic sphagnum bogs, or ditches (Price et al., 2016).

In land plants, largely represented in research by the model plant *Arabidopsis thaliana*, the processing of environmental signals into cellular responses is needed for stress adaptation.

These signaling mechanisms are well described, and research is primarily motivated by the need for agricultural innovations by creating new crop varieties able to cope better with a constantly changing environment. Notably, studying how plants use small molecule hormones called "phytohormones" to coordinate developmental processes and stress responses leads to a complex but still incomplete model describing ways to induce plants to sustain growth even under biotic and abiotic stresses.

Hormone signaling is poorly understood in primary plastid-bearing algae, which share a common ancestor with land plants, including crops. Hormone research in algae mainly focuses on green algae, with *Chlamydomonas reinhardtii* used as a model species, and a few other green algal species with commercial potential. To extend our knowledge of hormone signaling in Archaeplastida, we tested hormone production and responses in the glaucophyte *Cyanophora paradoxa*. Iconic phytohormones with a significant role in coordinating land plant developmental and environmental signaling and responses include salicylic acid (SA), jasmonic acid (JA), abscisic acid (ABA), ethylene (ET), auxins (AUXs), cytokinins (CKs), gibberellic acid (GA), and brassinosteroids (BRs). From algal genomes, including that of *C. paradoxa*, it is yet impossible to predict whether a given hormone might play an active role in the cell. This is in part because the biosynthesis genes, receptors, and downstream effectors of phytohormones often have little to no apparent homology between well-described land plant versions and genes in distantly related algae (Bidon et al., 2020). Even when homology can be inferred, the binding of specific molecules to the algal proteins and the resultant downstream protein-protein interactions cannot yet be computationally predicted accurately in novel contexts (Evans et al., 2022; Mou et al., 2021). One well-known hormone in plants is ethylene (C_2H_4), the only gaseous molecule described as an active phytohormone (Schaller and Kieber, 2002). In plants, ethylene plays various but essential roles in both stress responses and development (Binder, 2020). It has been intensely studied in the model plant *Arabidopsis* for the last 20 years since the discovery of the first ethylene-insensitive mutant (Thomma et al., 1999). In crops, it can control fruit ripening and is used in postharvest storage control (Cocetta and Natalini, 2022)

Ethylene synthesis is well described and requires only a few steps from the initial amino acid methionine. The first step is the production of S-adenosyl-L-methionine (SAM) from methionine by the enzyme SAM synthetase (SAMS). SAM is a vitally important molecule for

methylation processes in cells but is also an essential ethylene precursor. In ethylene signaling, SAM is converted into 1-aminocyclopropane-1-carboxylic acid (ACC) by ACC-synthase (ACS). The final step involves the enzyme ACC-oxidase (ACO), which converts ACC to gaseous C_2H_4. ACS activity is considered the rate-limiting step of ethylene biosynthesis (Van de Poel and Van Der Straeten, 2014). Therefore, the ACS product and direct ethylene precursor ACC, which is water soluble, is frequently applied in controlled experiments to trigger ethylene synthesis and investigate its downstream effects (Adams and Yang, 1979; Li and Guo, 2018; Park et al., 2023).

Although it is often regarded as a phytohormone, primarily understood for its roles in plant development and stress responses, ethylene production has also been observed outside the plant kingdom (Tsavkelova et al., 2006). At least four biological mechanisms are known for ethylene production: the recently discovered mechanism via (2-methylthio)-ethanol in soil bacteria (North et al., 2020), via 2-oxoglutarate in bacteria and fungi (Herr and Hausinger, 2018), via 2-keto-4-methylthiobutyric acid (KMBA) in bacteria and fungi (Nazli et al., 2003), and via the abovementioned 1-aminocyclopropane-1-carboxylate (ACC) in plants (Pattyn et al., 2021). Among photosynthetic algae, comparative genomic analyses found homologs of the ethylene biosynthesis genes *ACS* and *ACO*, as well as homologs of the plant signal transduction genes ETHYLENE RESPONSE 1 (*ETR*) and CONSTITUTIVE TRIPLE RESPONSE 1 (*CTR1*) in Zygnematophyceae, the algal lineage sister to land plants, with additional evidence of homologs in unicellular chlorophyte algae like *Chlamydomonas reinhardtii* (Feng et al., 2023). Additionally, zygnematophyte algae can produce ethylene when provided with exogenous ACC (Ju et al., 2015). Moreover, ethylene production has been observed in the chlorophyte green algae *Chlamydomonas reinhardtii* and *Haematococcus pluvialis* (Maillard et al., 1993; Yordanova et al., 2010) and the red algae *Pterocladiella capillacea* and *Gelidium arbuscula* (Garcia-Jimenez et al., 2013). While these studies point to a common ancient origin of ethylene synthesis and responses in Archaeplastida algae, a demonstrable recent divergence of plant ethylene synthesis genes (D. Li et al., 2022) and innovations in ethylene signal transduction (Mao et al., 2022) make it difficult to identify the precise origins and evolution of ethylene signaling.

For this study, we considered ethylene synthesis and downstream responses in the glaucophyte alga *Cyanophora paradoxa*. We observed a native production of ethylene after

stress, the conversion of the plant ethylene precursor ACC to ethylene, and some transcriptional responses shared between glaucophytes and plants. Our experimental investigation of ethylene responses allows us to extend our functional knowledge of ethylene signaling to the last common ancestor of the Chloroplastida and Glaucocystophycea.

Material and methods

Algae strain and culture

C.paradoxa CCMP329 was used for this study. Cells were cultivated in a modified AF6 media at 16°C in a Percival culture chamber with 12 hours of daylight (40 µE/m^2/s). Modified AF6 media was made without ammonia but with 3.85 mM $NaNO_3$ and trace metals following Kropat et al. (2011).

ACC treatment

ACC (1-aminocyclopropane-1-carboxylic Acid - Sigma 149101) was solubilized in water (200 mM stock) and used to treat *C. paradoxa* cells in the following experiments at the mentioned concentrations.

Gas Chromatography-Flame Ionization Detector (GC-FID)

For this experiment, 15 mL of *C. paradoxa* cells in culture media were sealed for 48 hours in 15 mL headspace vials with appropriate treatments. Ethylene concentrations in the headspace air (2 mL) were determined by gas chromatography. The SRI 8610C gas chromatograph was equipped with a flame ionization detector (GC-FID) and a 3' x $^1/_8$" HAYESEP D packed column. Headspace gas was injected into the column through a 1000 µL sample loop, with N_2 as the carrier gas at a flow rate of 15 mL/min, and the flame gases H_2 and air at 25 and 250 mL/min, respectively. The isothermal column oven temperature program was set at 50ºC. Under these conditions, ethylene retention time was ~2.466 minutes. A commercial ethylene standard (GASCO, USA, 2 ppm C_2H_4 in N_2), diluted sequentially in air, was used to generate the calibration of ethylene concentration and peak area. Cell concentration was determined using a hemocytometer, and results were expressed as ng ethylene/10^6 cells measured from the 1 mL headspace of the vials. All experiments were repeated three times using the same conditions.

Experimental treatments: Stress response and ABA treatment

Flg22 peptide (RP19986, GenScript) was solubilized in water and used at a final concentration of 100 nM. $CuCl_2$ (Sigma 307483) was solubilized in water and used at a final concentration of 10 µM. For osmotic shock, cells were pelleted at 500 g for 5 minutes and resuspended in 5 mL AF6 media supplemented with 0.1 M sucrose. After 15 minutes of incubation at 16°C, cells were pelleted again and resuspended in 15 mL fresh AF6 media. For UV-B exposure, cells were incubated 2 hours in a dark box containing a UVB100 (ExoTerra) lamp providing about 115 $\mu W/cm^2$ UV-B radiations (from the manufacturer's manual). ABA (Sigma 862169) was solubilized in DMSO and used at a final concentration of 100 µM.

Hydrogen peroxide quantification and visualization

Hydrogen peroxide in *C.paradoxa* cells was quantified using the ROS-Glo H_2O_2 assay (Promega). 20 mL cultures were treated with different ACC concentrations or a mock (water) and incubated for three days in a culture chamber. Cells were then pelleted for 5 minutes at 500 g and resuspended in 200 µL AF6 media. For each condition, 40 µL resuspended cells quadruplicates were used. The ROS-Glo assay was then conducted following the manufacturer's instructions, and results were acquired on a Filter-max-F5 plate-reader (Molecular Devices). For ROS visualization in live cells, CellROX Green Reagent (Invitrogen) was used following the manufacturer's instructions. Cells were observed using a Leica DMi8 inverted epifluorescence microscope. ROS were visualized using excitation at 480 nm and a 510 nm emission filter and captured with a DFC9000 sCMOS camera. The green color was quantified using ImageJ software (n = 40 cells for each condition). All experiments were repeated three times using the same conditions.

RNA extraction

RNA extraction for RNAseq was achieved using a combination of TRIzol (Invitrogen) and PureLink RNA Mini kit (Invitrogen). *C. paradoxa* cells were pelleted at 600 g for 10 minutes. Subsequently, the cells were lysed in 1 mL TRIzol, and the aqueous phase was separated by adding 0.2 mL chloroform, followed by centrifugation at 12000 g for 5 minutes. The resulting aqueous phase, containing the cell lysate, was loaded onto a PureLink RNA Mini kit column.

The RNA extraction was then conducted according to the instructions provided by the manufacturer, yielding purified RNA samples for further analysis.

RNAseq analyses

Total RNA was submitted to a sequencing facility, Genewiz (Azenta, South Plainfield, NJ), for short-read sequencing on the Illumina HiSeq platform. Poly-A selection was completed prior to library prep at the facility, and cDNA library sequencing was completed with 2 x 150 bp paired-end reads per fragment/template. Sequencing generated an average of 23,645,698 read pairs per sample with triplicate samples per condition. Reads were aligned to the *C. paradoxa* reference transcriptome derived from the reference genome (Price et al., 2019) (Transcriptome file: *Cyanophora paradoxa* CCMP329: Cyapar1_GeneCatalog_transcripts_20200807.nt.fasta.gz) using the program Salmon (v1.1.0) (Patro et al., 2017) with decoys generated from the genome assembly. Quantitative differential expression analyses were performed in R (R Core Team, 2013). Salmon quantification files were imported using the function "tximport" (Soneson et al., 2015). Differential expression was completed with edgeR (v3.40.2) using a generalized linear model, a fold-change cutoff of 1.5, and an FDR of 0.05, such that a DE gene had to be 1.5 times over- or under-expressed compared to the control with an FDR < 0.05 in order to register as differentially expressed. For functional analyses, proteins were re-annotated using the most recent version of InterPro (interproscan v5.59-91.0) (Paysan-Lafosse et al., 2023), and gene ontology (GO) terms assigned by interproscan were used for functional enrichment analyses using the program topGO (v2.50.0; GO.db v3.16.0) (Alexa A, Rahnenfuhrer J, 2023). Enrichment analyses were visualized with GOplot (Walter et al., 2015).

Protein structure prediction

The amino acid sequence of *C. paradoxa* peptide g9335.t1 was compared to other 2OGD proteins selected from the literature or BLAST searches by alignment using Mafft (v7.520) (Katoh and Standley, 2013). Protein structural prediction was performed using AlphaFold2 ColabFold online notebook (v1.5.2-patch: AlphaFold2 using MMseqs2) (Mirdita et al., 2022). Structural analyses and backbone alignment were performed in the online Mol* viewer (Sehnal et al., 2021) hosted at rcsb.org.

RESULTS

C. paradoxa converts ACC into gaseous ethylene

The conversion of ACC to ethylene is a hallmark of plant ethylene synthesis. Exposing plants to exogenous ACC induces the production of ethylene gas (Zhang and Wen, 2010) and the activation of ethylene signaling (Park et al., 2023). To probe whether glaucophyte algae use a plant-like ethylene synthesis mechanism, we added the plant ethylene precursor ACC to *C. paradoxa* cultures and measured ethylene production by GC-FID. *C. paradoxa* cells treated with ACC produced ethylene, while mock-treated samples did not (Figure 1A). Levels of produced ethylene corresponded to the concentration of added ACC; 0.5, 1, and 5 mM ACC treatments corresponded led, respectively, to 49, 137, and 283 ng ethylene/10^6 cells measured in the headspace of the vials, on average. These data indicate that *C. paradoxa* cells can convert ACC into gaseous ethylene, suggestive of a plant-like ethylene signaling pathway in glaucophytes.

C. paradoxa makes ethylene natively in response to abiotic stress

As a plant hormone, ethylene is known to regulate plant growth and specific developmental processes (Schaller and Kieber, 2002). It also acts in response to various biotic and abiotic stresses, such as pathogen invasion (Broekaert et al., 2006), chewing insects (von Dahl and Baldwin, 2007), UV-B stress (He et al., 2011), heavy metal stress (Keunen et al., 2016), and osmotic stress (Tao et al., 2015). To test whether *C. paradoxa* cells produce ethylene in response to stresses, *C. paradoxa* cultures were exposed to the synthetic peptide flg22, which mimics bacterial invasion in plants (Meindl et al., 2000), UV-B, $CuCl_2$ oxidative stress, and sucrose-induced osmotic shock. All evaluated abiotic stress conditions (Figure 1B) elicited ethylene production by *C. paradoxa* cultures (~ 60 ng/10^6 cells measured in the headspace of the vials, on average) except the candidate biotic stressor, flg22. These results indicate that ethylene synthesis by *C. paradoxa* cells is induced in response to abiotic stress, in agreement with plant stress responses, but not by the biotic stressor flg22, in contrast to plants.

ROS accumulation occurs following abiotic stress and ACC treatment in *C. paradoxa.*

Reactive Oxygen Species (ROS) are common second messengers in signaling pathways, accumulating in response to stress or perception of signaling molecules and contributing to downstream effects within a cell by amplifying the primary signal and activating additional effectors (Schieber and Chandel, 2014). In plants, abiotic stress and ethylene pathway activation are known inducers of ROS accumulation, which is followed by downstream responses like the hypersensitive response, a rapid cell death mechanism aiming to prevent pathogens infections, and/or programmed cell death.

We tested whether abiotic stresses or ACC exposure, both of which induce ethylene production, was followed by ROS accumulation in *C. paradoxa* cells by quantifying hydrogen peroxide (H_2O_2) content following the treatment (Figure 2A). Osmotic shock and UV-B stress caused a significant increase ($p < 0.05$, Student's *t*-test) of 8 and 1.6 fold, respectively, in the H_2O_2 content of *C. paradoxa* cells. Copper-treated cells had a slight, but not statistically significant, 1.1-fold increase in H_2O_2 content ($p = 0.06$, Student's *t*-test).

Treatment of *C. paradoxa* cells with ACC (Figure 2B) induced a significant accumulation of H_2O_2 ($p < 0.05$, ANOVA) at treatment concentrations of 1 mM and 5 mM, and the H_2O_2 content of the cultures positively corresponded to the ACC dosage. We also visualized ROS accumulation (Figure 2C) in *C. paradoxa* cells following ACC treatment using CellRox, a ROS-specific dye. The addition of 1 mM ACC resulted in multiple ROS foci spread through the cells 24 hours after treatment. Quantification of CellRox fluorescence intensity (Figure 2D) revealed significantly higher ROS content in ACC-treated algae ($p < 0.05$; Student's *t*-test) compared to controls.

ACC treatment causes growth inhibition of *C. paradoxa*

In plants, one major physiological response to the perception of ethylene is the suppression of growth in root and shoot epidermis cells (Vaseva et al., 2018). One reason for growth suppression may be the conservation of resources during stress (Huot et al., 2014). If *C. paradoxa* perceives ethylene as a stress signal, it could similarly enter a resource conservation mode and slow or stop growth. Therefore, we tested the effect of ACC treatment on the growth of *C. paradoxa* (Figure 3). The growth of *C. paradoxa* cultures was monitored during continuous

exposure to ACC. Cultures exposed to 1 mM or more ACC exhibited significant growth inhibition by day 5 ($p < 0.05$, ANOVA) (Figure 1B). Importantly, when ACC was removed from growth-inhibited cultures, growth resumed, indicating that the growth inhibition is reversible (Suppl. Figure 1).

ABA interacts with ACC/ethylene signaling in *C. paradoxa.*

In accordance with findings that ABA, a second major phytohormone, perception and signaling systems exist within algae (Sun et al., 2020), we explored the potential for crosstalk between ABA and ethylene signaling in *C.paradoxa*. In plants, ABA often suppresses ethylene signaling activities (Dong et al., 2016).

Cells treated simultaneously with ABA and ACC and assayed 24 hours later exhibited reduced ethylene production by about 50% compared to cells treated with ACC only, indicating that ABA negatively regulates ethylene synthesis in *C. paradoxa* (Figure 4A). Individual treatments with either ACC or ABA induced H_2O_2 production to similar levels ($p > 0.05$, ANOVA) (Figure 4B). Dual treatment with ABA and ACC exhibited an additive effect, with significantly increased H_2O_2 accumulation compared to the single treatments ($p < 0.05$, ANOVA). These results indicate that crosstalk between ethylene and ABA signaling occurs in *C. paradoxa*, further supporting the notion that glaucophytes and green plant signaling modalities share similar features.

ACC treatment induces upregulation of senescence-associated proteases in *C. paradoxa*

One output of signal transduction is the alteration of gene expression levels in response to a specific signal or stress. To reveal the glaucophyte response to ACC/ethylene and compare it to that from specific stressors, we conducted RNAseq experiments (Figure 5, Suppl. File 1) to identify differentially expressed genes (DEG) in response to ACC and abiotic stresses (UV-B, osmotic stress, and Cu-induced oxidative stress). After 24 hours of treatment, ACC treatment induced a small number of transcriptional changes, 37 DEGs (28 up and 9 down), despite having large effects on growth (e.g., Figure 3). A low level of copper exposure induced a similarly low number of DEGs (10 up and 4 down). In contrast, cells exposed to abiotic stress exhibited high

numbers of DEGs (774 up and 1568 down) 24 hours after a 2-hour UV-B stress and 833 DEGs (388 up and 445 down) after a 15-minute osmotic stress.

Functional enrichment analysis of DEGs (Figure 6, Suppl. File 2) revealed that the top enrichment category for cells exposed to osmotic stress and UV-B was iron ion transmembrane transport. However, the direction of change was different for the two stresses; genes associated with iron ion transmembrane transport were upregulated after osmotic stress and downregulated after UV-B stress. One process induced by hyperosmotic stress is vacuolar transport, a response similar to that of plants (Zwiewka et al., 2015). Notably, UV-B stress was associated with the upregulation of RNA-pol I, the RNA polymerase responsible for the transcription of ribosomal genes, and double-strand break repair, while it was associated with the downregulation of key photosynthetic processes.

ACC treatment was associated with a small number of transcriptional changes. Nevertheless, the differentially expressed genes did coalesce around three functional categories: proteolysis, t-RNA splicing, and microtubule polymerization. Similarly, treatment with copper had two enrichment categories: proteolysis and microtubule polymerization.

Discussion

In this study, we showed that *C. paradoxa*, a primary plastid-bearing alga within the glaucophyte group, produces the hormone ethylene when provided with the plant-like precursor molecule ACC and natively in response to abiotic stress. Additionally, *C. paradoxa* responds to the hormone ABA with evidence of crosstalk between ABA and ethylene signaling. This is the first report of hormone usage in a glaucophyte alga, extending our knowledge of hormone usage for the coordination of stress responses to the base of the Archaeplastida.

Prior research indicates an early origin of ethylene detection in Archaeplastida, with ethylene receptors likely acquired from a cyanobacterial symbiont, the precursor of the plastid (Gamble et al., 1999). However, the plant-like pathway for ethylene synthesis, using the precursor molecule ACC, appears to have a more recent evolutionary origin (Li et al., 2018; X. Li et al., 2022). This theory is supported by the absence of ACC oxidase genes in non-seed-

bearing plants (non-spermatophytes) and an apparent inability of non-spermatophytes to convert ACC to ethylene (Li et al., 2018; X. Li et al., 2022). Evidence challenging the hypothesis that ACC-based ethylene synthesis originated recently (i.e., in spermatophytes) comes from observations of ACC conversion to ethylene in green and red algae. The charophyte alga *Spirogyra pratensis* converts ACC to ethylene and is reported to have ethylene synthesis and response systems homologous to the land plant version (Ju et al., 2015). Likewise, the green alga *Haematococcus pluvialis* makes ethylene upon ACC exposure (Maillard et al., 1993), and the red alga *Pterocladiella capillacea* produces ethylene natively and reportedly converts ACC into ethylene with an ACO-like activity (García-Jiménez and Robaina, 2012). Given the newly presented evidence of ACC-to-ethylene conversion in a glaucophyte alga, the origins of a plant-like ethylene synthesis and response pathway might be pushed back to the base of the Archaeplastida lineage.

The *ACO* gene in plants encodes a 2-oxoglutarate and Fe (II)-dependent dioxygenase domain (2OGD)-containing protein (Kawai et al., 2014). Using the tomato *Solanum lycopersicum* ACO4 protein sequence (UniProt P24157) as a seed to search available genomes, we found that *C. paradoxa* has three recognizable homologs of 2OGD proteins at an e-value cutoff of 10^{-10}; the genes are candidates for ethylene synthesis activity in glaucophytes. The green alga *H. pluvialis* encodes two, the charophyte alga *Closterium sp.* encodes one, and the unicellular red alga *Porphyridium purpureum* encodes one. The apparent recent origins of the gene encoding ACO in spermatophytes may be due to the explosive expansion of the 2OGD gene family in embryophytes (land plants) with the non-vascular moss *Physcomitrella patens* encoding 77 2OGD proteins, the model lycophyte *Selaginella moellendorffii* encoding 134, the model plant *A. thaliana* encoding over 150 2OGD proteins, and the tomato *Solanum lycopersicum* encoding 131 divided into seven distinct clades (Wei et al., 2021). The relatively recent expansion of that gene family in embryophytes may have obscured the ancient origins of ethylene synthesis via ACC. The seed plant *ACO* gene family likely has a recent origin corresponding to the base of the spermatophytes. However, that does not exclude the possibility that other ancient 2OGD proteins can complete ACC oxidation into ethylene.

Considering the active site of the plant, ACO crystallized with the substrate ACC (PDB 5TCV) (Berman et al., 2003) and a *de novo* predicted fold of *C. paradoxa* 2OGD protein

g9335.t1 key residues are in identical locations (Figure 7A), even though the proteins only exhibit a 24% identity. One intriguing similarity is that plant ACOs do not bind 2-oxoglutarate and, indeed, have an alteration in a key residue used to stabilize 2-oxoglutarate in other 2OGD proteins. 2OGD proteins that bind 2-oxoglutarate, like the *A. thaliana* jasmonate-induced oxygenase (JOX2, PDB structure 6LSV), have an asparagine residue that forms a hydrogen bond with a carboxylate oxygen of 2OG (Figure 7B) (Zhang et al., 2021). Plant ACOs have a serine at the indicated position, while one of the glaucophyte 2OGD proteins has a leucine, neither of which can form a hydrogen bond with 2-oxoglutarate (Figure 7C). The amino acid difference may allow greater substrate flexibility in the active site for a molecule like ACC. This possibility is exemplified by a putative ACC oxidase protein from the amoebozoan *Dictyostelium mucoroides*. The *D. mucoroides ACO* gene is necessary and sufficient for ethylene production by the amoebozoan (Amagai et al., 2007). Residues in the active site of the corresponding protein are organized like the *C. paradoxa* 2OGD protein (Figure 7), suggesting that the *C. paradoxa* protein, and others like it, may be capable of ACC oxidation to ethylene. Alternatively, glaucophytes and other algae might not use 2OGD proteins for the conversion of ACC to ethylene at all. Future experimental testing is needed to determine the mechanism of ACC to ethylene conversion observed in green, red, and glaucophyte algae.

Downstream of ACC, which induces ethylene production, we see responses in *C. paradoxa* that mirror some plant responses to stress and ACC/ethylene signaling, such as ROS production and entrance into a quiescence-like state where cell division is inhibited in a reversible fashion and growth can resume once the signal is removed. Halting division is a common stress response in plants and other organisms (Hill et al., 2014; Qi and Zhang, 2020; Sun and Gresham, 2021), presumably as a means to conserve resources and/or avoid damage when organisms are under conditions they are not adapted to. Compared to the broad stress response of *C. paradoxa* to UV and osmotic stress, the response to ACC at the level of gene regulation is minimal, with only 28 upregulated and 9 downregulated genes (Figure 8). That small number of differentially expressed genes, however, has a large apparent effect on the organism. Key genes and protein domains whose expression changes in *C. paradoxa* cells exposed to ACC include an upregulated homolog of the atypical protein kinase RIO1. In the yeast *Saccharomyces cerevisiae*, the protein RIO1 is required for cell cycle progression (Angermayr et al., 2002), and the protein is known to interact with the ribosome, influencing

translation (LaRonde-LeBlanc and Wlodawer, 2005). Moreover, a *RIO1* homolog was identified as an upregulated gene under elevated pH, a condition associated with decreased growth, in the diatom *Fragilaria crotonensis* (Zepernick et al., 2022). It is not clear how the upregulation of a protein kinase needed for cell cycle progression influences the observed growth arrest. However, given the specificity of the response to ACC, RIO1 likely plays a significant role in the observed effect. Another upregulated gene encodes an AN1 zinc-finger domain-containing protein known to be involved in stress responses in plants and animals (Vij and Tyagi, 2008). Additionally, a gene encoding Multiprotein Bridging Factor 1 (MBF1) protein was upregulated following ACC exposure. *MBF1* is induced during the plant response to stress (Jaimes-Miranda and Chávez Montes, 2020) and is a bridging factor between transcription factor binding and transcription start sites. At last, four genes encoding subtilisin-like serine proteases (subtilases) were found upregulated. Subtilases have roles in plant biotic and abiotic stress responses and development (Berger and Altmann, 2000; Figueiredo et al., 2017; Schaller et al., 2012). In *C. paradoxa*, the upregulated subtilases may act as general proteases or through specific mechanisms to regulate the cell cycle.

Although ACC exposure has a clear effect on cell division, there is no apparent change in the expression of cyclins at the examined time point (Suppl. Figure 2). This observation contrasts with UV and osmotic stress, which both affect the expression of cyclins, sometimes in opposite directions, with likely effects on cell cycle progression, leading to cells being at different stages of the cell cycle while they recover from the stress (Suppl. Figure 2). For example, Cyclin A2 is downregulated in sucrose-exposed cells at 24 hours but unchanged in UV-exposed cells with respect to the untreated control, suggesting that cells after hyperosmotic stress are not in the S/G2 phase of the cell cycle at the tested time point (Suppl. Figure 2B). Cyclin B2, however, is highly upregulated in UVB-exposed cells and relatively downregulated in sucrose-exposed cells (Suppl. Figure 2B), suggesting that the UVB-exposed cells may be undergoing mitosis at 24 hours, a hypothesis that can be tested in future studies. How the quiescent state is maintained in ACC-exposed cells without changes in expression to cyclin genes compared to the control is not known, though it would be interesting to track control and ACC-exposed cells through time to further examine the role of the cell cycle with respect to the quiescent state induced by ACC.

In addition to the effects of ACC and a presumed ethylene-like signaling pathway, we observed an effect of ABA on ROS production and an additive effect when cells were exposed to both ACC and ABA. However, ABA caused a decrease in the conversion of ACC to ethylene, which could suggest either a decoupling of ACC, ethylene, and ROS production or that the ACC/ethylene concentration was still high enough to have an additive effect. Additional experiments are needed to determine how hormonal crosstalk operates in glaucophytes. One possibility is that ACC operates as a signal on its own, independent of ethylene. ACC, as a signaling molecule decoupled from ethylene signaling, has been observed in several plants with various effects, such as halting cell division and altering cell morphology (X. Li et al., 2022). We see robust ethylene production upon ACC exposure in *C. paradoxa*, but further research is needed to discover how ACC and ethylene signaling might operate in concert or independently in glaucophytes.

In conclusion, our study on the glaucophyte *C. paradoxa* provides valuable insights into the evolutionary origins of ethylene synthesis and signaling pathways, revealing conserved molecular mechanisms that may extend beyond glaucophytes and land plants (Figure 9). The study adds mechanistic insight to the observation that abiotic stress responses are conserved between plants and glaucophytes (Ferrari and Mutwil, 2020) by showing that stress responses may be enacted through conserved hormone signaling pathways. Future studies should aim to identify the specific genes involved in ethylene synthesis and signaling in glaucophytes and explore the potential presence and function of other hormone pathways in other eukaryotes. By doing so, we can gain a more comprehensive understanding of the role and conservation of hormone signaling in the coordination of stress responses and growth regulation across diverse eukaryotes, further our knowledge of the complex interplay between these signaling pathways that have evolved to adapt to various environmental conditions, and establish more robust connections between genomic information and cellular behavior, ultimately developing our understanding of the intricate relationship between genotype and phenotype.

Data Availability

A mapped read count table for all transcriptome data and the protein structure (.pdb) file from the best Alphafold2 prediction for the glaucophyte 2OGD peptide are available as

supplemental data with this manuscript. All raw RNAseq reads were deposited at the NCBI SRA under BioProject #PRJNA979222.

Acknowledgment

This work was funded in part by the National Science Foundation OIA-1826734. M.G. and M.Y. were supported by a National Science Foundation Research Experience for Undergraduates program at Bigelow Laboratory (NSF EAR 1460861).

Competing interests

No competing interests were declared.

Figure legends

Figure 1: *C. paradoxa* cultures convert ACC to ethylene and produce ethylene natively after stress

Ethylene measurements from *C.paradoxa* cultures using gas chromatography (GC-FID). Results are expressed in ng/ethylene/million cells as measured from the air in the headspace of the vials. To obtain ethylene quantities, the peak area was measured, and ethylene concentrations were determined using a commercial ethylene (Gasco) standard. (A) Samples were treated with ACC before being incubated in sealed vials (n = 4 for each treatment) for gas chromatography. All ACC-treated samples displayed significant ethylene production (*$p < 0.05$, ANOVA) compared to mock (water) samples. (B) Samples were either treated with 100 nM flg2 or 10 µM CuCl2, exposed to UV-B for 2 hours, or shocked in 0.1 mM sucrose for 15 minutes before being incubated in sealed vials for gas chromatography (n = 3 for each treatment). Asterisks (*) indicate significant ethylene production (*$p < 0.05$, ANOVA) compared to mock (water) treatment.

Figure 2: Hydrogen peroxide accumulation is induced downstream of stress and ACC treatments by *C. paradoxa*

(A) Hydrogen peroxide assay (ROS-GLO). Cells were treated the same way as in Figure 1B but were incubated in a culture chamber for 16 hours before being collected for the ROS-GLO assay (n = 4 for each condition). Asterisks (*) indicate significantly higher hydrogen peroxide compared to control cells (* $p < 0.05$, Student's t-test). RLU = Relative Light Units.

(B) Cells were treated with different ACC concentrations and were incubated in a culture chamber for 24 hours before being collected for the ROS-GLO assay (n = 4 for each condition). Asterisks (*) indicate significantly higher hydrogen peroxide compared to control cells (*p < 0.05, ANOVA). RLU = Relative Light Units.

(C) Fluorescence micrographs of *C.paradoxa* cells treated with 1 mM ACC and CellRox dye allowing ROS visualization. Pictures were taken 24 hours after treatments. Scale bar = 9 µm. Left panel: Control cells; Right panel: ACC-treated cells. Fluorescence channels: Red (Chlorophyll) Ex/Em 650/700 nm; Green (CellRox) Ex/Em 485/520 nm. ACC 1mM (Zoom) picture panel: Detailed view of a *C.paradoxa* cell treated with 1 mM ACC. Upper left: bright field; Upper right: chlorophyll autofluorescence; Bottom left: Cell Rox (ROS); Bottom right: merge of all channels. Green signal quantification per cell measurements was made using ImageJ.

Figure 3: ACC treatment causes growth inhibition of *C. paradoxa* cultures

C.paradoxa cell concentrations over 5 days after ACC treatments. 20 mL cultures of *C.paradoxa* were treated with ACC or mock (water) and incubated in a culture chamber for 5 days. Cell concentrations were monitored on days 0, 3, and 5 using a hemocytometer. Asterisks (*) indicate a significant difference compared to control cells at the appropriate time point (*p < 0.05, ANOVA).

Figure 4: Crosstalk between ACC and ABA signals in *C. paradoxa*

(A) Ethylene measurements using a gas chromatography setup (GC-FID). Results are expressed in ng/ethylene/million cells. Samples were either treated with mock (DMSO), 100 µM ABA, 1 mM ACC, or a combination of ACC and ABA before being incubated in sealed vials for gas chromatography (n = 3 for each condition). (*) indicates a significant difference (*p < 0.05, ANOVA) compared to the mock treatment. (**) indicates a significant difference between mock and ACC conditions. (B) Hydrogen peroxide assay (ROS-GLO). Cells were treated with different ACC or ABA concentrations and incubated in a culture chamber for 24 hours before being collected for the ROS-GLO assay (n = 3 for each condition). (*) indicates a significant difference (*p < 0.05, ANOVA) between the two conditions. ns: non-significant differences (p > 0.05, ANOVA). RLU = Relative Light Units.

Figure 5: Transcriptional changes after abiotic stress and ACC treatments in *C. paradoxa*

Differentially expressed genes in *C. Paradoxa* after abiotic stresses (UV-B, osmotic, and oxidative) and 1 mM ACC treatments. Mean-difference plots (Log fold change vs. Average log CPM) show genes significantly differentially expressed (FDR < 0.05) with a log fold change < log2 (1.5). Upregulated genes are highlighted in red, and downregulated genes are highlighted in blue.

Figure 6: Functional characterization of differentially expressed genes following abiotic stress and ACC treatment

(A) Gene ontology circle plots (GO plots) showing the top significantly enriched GO terms associated with Biological Processes (BP) for differentially expressed genes following abiotic stress. (B) Table displaying the significantly enriched GO terms after ACC treatment.

Figure 7: Structural characterization of a *C. paradoxa* 2OGD protein

(A) Multiple alignment of 2OGD proteins, including proteins that use 2OG as a co-substrate, canonical ACC oxidases that do not use 2OG, and other 2OGD proteins that may have reduced affinity for 2OG based on an amino acid difference at the highlighted position: Asp (N) in 2OGD proteins known to bind 2OG; Ser (S) in ACOs; Leu (L) in other 2OGDs, including a *C. paradoxa* protein and an amoebozoan (*Dictyostelium mucoroides*) 2OGD protein known to act as an ACC oxidase. (B) Organization of residues that contact the 2OG co-substrate in the *A. thaliana* protein jasmonate-induced oxygenase 2 (JOX2) from PDB crystal structure 6LSV. Hydrogen bonds are indicated as dashed lines. The pink arrowhead indicates the hydrogen bond that is lost when N227 of 2OG binding proteins like JOX2 is replaced with Ser as in ACOs or Leu as in other 2OGD proteins. Species abbreviations: Athal = *A. thaliana*, Cyapar1 = *C. paradoxa*, Ceust = *Chlamydomonas eustigma*, Scen = *Scenedesmus* sp. NREL 46B-D3, Oquek = *Ostreobium quekettii*, Maldo = *Malus domestica*, Osat = *Oryza sativa*, Slyc = *Solanum lycopersicum*, Pxhyb = *Petunia hybrida*, Chlam.sp = *Chlamydomonas* sp. UWO 241, Crein = *Chlamydomonas reinhardtii*, Pico.sp = *Picochlorum* sp. BPE23, Clos.sp = *Closterium* sp. NIES-68, Smoel = *Selaginella moellendorffii*, Rmar = *Rhodosorus marinus*, Dmuc = *D. mucoroides*. (C) Overall fold structure and active site organization of a *Petunia hybrida* ACO crystallized with substrate ACC, PDB ID: 5TCV, and a *de novo* fold prediction for a predicted *C. paradoxa* 2OGD protein from gene g9335.t1, and a structural alignment of the two. Active site residues (H177, D179, H234 of 5TCV; H220, D222, H276 of *C. paradoxa* g9335.t1) are shown as ball and stick representations; a metal co-factor, Ni (Fe in the active complex), from 5TCV is also shown as a green ball. Hydrogen bonds between active site residues and the ACC substrate are shown as dashed lines for 5TCV.

Figure 8: Heatmap of relative expression levels of differentially expressed transcripts associated with ACC treatment across all treatments of *C. paradoxa*.

The heatmap shows how genes associated with ACC/ethylene signaling are expressed in control cells and after other treatments. Some expression patterns are shared, while others differ/are unchanged compared to the control in other treatments. Genes discussed in the text are highlighted in yellow (indicated aqualysins and serine proteases are subtilases).

Figure 9: Preliminary model of ethylene signaling in *C. paradoxa*

Schematic representation of the main results of this study. Molecules known as phytohormones are represented in red. Plain black links refer to direct experimental results from this work. Dashed black links represent possible connections in the cell signaling pathway of *C. paradoxa*. Gray dashed links represent the hypothetical positive regulation of ethylene on ABA that could lead to a negative feedback control mechanism based on our results (e.g., Figure 4A).

References

Adams, D.O., Yang, S.F., 1979. Ethylene biosynthesis: Identification of 1-aminocyclopropane-1-carboxylic acid as an intermediate in the conversion of methionine to ethylene. Proc. Natl. Acad. Sci. 76, 170–174. https://doi.org/10.1073/pnas.76.1.170

Alexa A, Rahnenfuhrer J, 2023. topGO: Enrichment Analysis for Gene Ontology. R package version 2.52.0.

Amagai, A., Soramoto, S.-S., Saito, S.-H., Maeda, Y., 2007. Ethylene induces zygote formation through an enhanced expression of zyg1 in Dictyostelium mucoroides. Exp. Cell Res. 313, 2493–2503. https://doi.org/10.1016/j.yexcr.2007.04.012

Angermayr, M., Roidl, A., Bandlow, W., 2002. Yeast Rio1p is the founding member of a novel subfamily of protein serine kinases involved in the control of cell cycle progression. Mol. Microbiol. 44, 309–324. https://doi.org/10.1046/j.1365-2958.2002.02881.x

Berger, D., Altmann, T., 2000. A subtilisin-like serine protease involved in the regulation of stomatal density and distribution in Arabidopsis thaliana. Genes Dev. 14, 1119–1131. PMID: 10809670 PMCID: PMC316574

Berman, H., Henrick, K., Nakamura, H., 2003. Announcing the worldwide Protein Data Bank. Nat. Struct. Mol. Biol. 10, 980–980. https://doi.org/10.1038/nsb1203-980

Bidon, B., Kabbara, S., Courdavault, V., Glévarec, G., Oudin, A., Héricourt, F., Carpin, S., Spíchal, L., Binder, B.M., Cock, J.M., Papon, N., 2020. Cytokinin and Ethylene Cell Signaling Pathways from Prokaryotes to Eukaryotes. Cells 9, 2526. https://doi.org/10.3390/cells9112526

Binder, B.M., 2020. Ethylene signaling in plants. J. Biol. Chem. 295, 7710–7725. https://doi.org/10.1074/jbc.REV120.010854

Broekaert, W.F., Delauré, S.L., De Bolle, M.F.C., Cammue, B.P.A., 2006. The role of ethylene in host-pathogen interactions. Annu. Rev. Phytopathol. 44, 393–416. https://doi.org/10.1146/annurev.phyto.44.070505.143440

Cocetta, G., Natalini, A., 2022. Ethylene: Management and breeding for postharvest quality in vegetable crops. A review. Front. Plant Sci. 13, 968315. https://doi.org/10.3389/fpls.2022.968315

Dong, Z., Yu, Y., Li, S., Wang, J., Tang, S., Huang, R., 2016. Abscisic Acid Antagonizes Ethylene Production through the ABI4-Mediated Transcriptional Repression of ACS4 and ACS8 in Arabidopsis. Mol. Plant 9, 126–135. https://doi.org/10.1016/j.molp.2015.09.007

Evans, R., O'Neill, M., Pritzel, A., Antropova, N., Senior, A., Green, T., Žídek, A., Bates, R., Blackwell, S., Yim, J., Ronneberger, O., Bodenstein, S., Zielinski, M., Bridgland, A., Potapenko, A., Cowie, A., Tunyasuvunakool, K., Jain, R., Clancy, E., Kohli, P., Jumper, J., Hassabis, D., 2022. Protein complex prediction with AlphaFold-Multimer. https://doi.org/10.1101/2021.10.04.463034

Feng, X., Zheng, J., Irisarri, I., Yu, H., Zheng, B., Ali, Z., Vries, S. de, Keller, J., Fürst-Jansen, J.M.R., Dadras, A., Zegers, J.M.S., Rieseberg, T.P., Ashok, A.D., Darienko, T., Bierenbroodspot, M.J., Gramzow, L., Petroll, R., Haas, F.B., Fernandez-Pozo, N., Nousias, O., Li, T., Fitzek, E., Grayburn, W.S., Rittmeier, N., Permann, C., Rümpler, F., Archibald, J.M., Theißen, G., Mower, J.P., Lorenz, M., Buschmann, H., Schwartzenberg, K. von, Boston, L., Hayes, R.D., Daum, C., Barry, K., Grigoriev, I.V., Wang, X., Li, F.-W., Rensing, S.A., Ari, J.B., Keren, N., Mosquna, A., Holzinger, A., Delaux, P.-M., Zhang, C., Huang, J., Mutwil, M., Vries, J. de, Yin, Y., 2023. Chromosome-level genomes of multicellular algal sisters to land plants illuminate signaling network evolution. https://doi.org/10.1101/2023.01.31.526407

Ferrari, C., Mutwil, M., 2020. Gene expression analysis of Cyanophora paradoxa reveals conserved abiotic stress responses between basal algae and flowering plants. New Phytol. 225, 1562–1577. https://doi.org/10.1111/nph.16257

Figueiredo, J., Sousa Silva, M., Figueiredo, A., 2017. Subtilisin□like proteases in plant defence: the past, the present and beyond. Mol. Plant Pathol. 19, 1017–1028. https://doi.org/10.1111/mpp.12567

Gamble, R.L., Coonfield, M.L., Randlett, M.D., Schaller, G.E., 1999. The Role of Two-Component Systems in Ethylene Perception, in: Kanellis, A.K., Chang, C., Klee, H., Bleecker, A.B., Pech, J.C., Grierson, D. (Eds.), Biology and Biotechnology of the Plant Hormone Ethylene II. Springer Netherlands, Dordrecht, pp. 59–64. https://doi.org/10.1007/978-94-011-4453-7_12

Garcia-Jimenez, P., Brito-Romano, O., Robaina, R.R., 2013. Production of volatiles by the red seaweed *Gelidium arbuscula* (Rhodophyta): emission of ethylene and dimethyl sulfide. J. Phycol. 49, 661–669. https://doi.org/10.1111/jpy.12083

García-Jiménez, P., Robaina, R.R., 2012. EFFECTS OF ETHYLENE ON TETRASPOROGENESIS IN PTEROCLADIELLA CAPILLACEA (RHODOPHYTA)1: ETHYLENE AND TETRASPOROGENESIS IN P. CAPILLACEA. J. Phycol. 48, 710–715. https://doi.org/10.1111/j.1529-8817.2012.01156.x

He, J., Yue, X., Wang, R., Zhang, Y., 2011. Ethylene mediates UV-B-induced stomatal closure via peroxidase-dependent hydrogen peroxide synthesis in Vicia faba L. J. Exp. Bot. 62, 2657–2666. https://doi.org/10.1093/jxb/erq431

Herr, C.Q., Hausinger, R.P., 2018. Amazing Diversity in Biochemical Roles of Fe(II)/2-Oxoglutarate Oxygenases. Trends Biochem. Sci. 43, 517–532. https://doi.org/10.1016/j.tibs.2018.04.002

Hill, A.J., Mansfield, R., Lopez, J.M.N.G., Raizen, D.M., Van Buskirk, C., 2014. Cellular stress induces a protective sleep-like state in C. elegans. Curr. Biol. CB 24, 2399–2405. https://doi.org/10.1016/j.cub.2014.08.040

Huot, B., Yao, J., Montgomery, B.L., He, S.Y., 2014. Growth–Defense Tradeoffs in Plants: A Balancing Act to Optimize Fitness. Mol. Plant 7, 1267–1287. https://doi.org/10.1093/mp/ssu049

Jackson, C., Clayden, S., Reyes-Prieto, A., 2015. The Glaucophyta: the blue-green plants in a nutshell. Acta Soc Bot Pol 17. http://dx.doi.org/10.5586/asbp.2015.020

Jaimes-Miranda, F., Chávez Montes, R.A., 2020. The plant MBF1 protein family: a bridge between stress and transcription. J. Exp. Bot. 71, 1782–1791. https://doi.org/10.1093/jxb/erz525

Ju, C., Van de Poel, B., Cooper, E.D., Thierer, J.H., Gibbons, T.R., Delwiche, C.F., Chang, C., 2015. Conservation of ethylene as a plant hormone over 450 million years of evolution. Nat. Plants 1, 14004. https://doi.org/10.1038/nplants.2014.4

Katoh, K., Standley, D.M., 2013. MAFFT Multiple Sequence Alignment Software Version 7: Improvements in Performance and Usability. Mol Biol Evol 30, 772–780. https://doi.org/10.1093/molbev/mst010

Kawai, Y., Ono, E., Mizutani, M., 2014. Evolution and diversity of the 2-oxoglutarate-dependent dioxygenase superfamily in plants. Plant J. Cell Mol. Biol. 78, 328–343. https://doi.org/10.1111/tpj.12479

Keunen, E., Schellingen, K., Vangronsveld, J., Cuypers, A., 2016. Ethylene and Metal Stress: Small Molecule, Big Impact. Front. Plant Sci. 7. https://doi.org/10.3389/fpls.2016.00023

Kropat, J., Hong-Hermesdorf, A., Casero, D., Ent, P., Castruita, M., Pellegrini, M., Merchant, S.S., Malasarn, D., 2011. A revised mineral nutrient supplement increases biomass and growth rate in Chlamydomonas reinhardtii. Plant J. Cell Mol. Biol. 66, 770–780. https://doi.org/10.1111/j.1365-313X.2011.04537.x

LaRonde-LeBlanc, N., Wlodawer, A., 2005. The RIO kinases: an atypical protein kinase family required for ribosome biogenesis and cell cycle progression. Biochim. Biophys. Acta 1754, 14–24. https://doi.org/10.1016/j.bbapap.2005.07.037

Li, D., Mou, W., Van de Poel, B., Chang, C., 2022. Something old, something new: Conservation of the ethylene precursor 1-amino-cyclopropane-1-carboxylic acid as a signaling molecule. Curr. Opin. Plant Biol. 65, 102116. https://doi.org/10.1016/j.pbi.2021.102116

Li, F.-W., Brouwer, P., Carretero-Paulet, L., Cheng, S., de Vries, J., Delaux, P.-M., Eily, A., Koppers, N., Kuo, L.-Y., Li, Z., Simenc, M., Small, I., Wafula, E., Angarita, S., Barker, M.S., Bräutigam, A., dePamphilis, C., Gould, S., Hosmani, P.S., Huang, Y.-M., Huettel, B., Kato, Y., Liu, X., Maere, S., McDowell, R., Mueller, L.A., Nierop, K.G.J., Rensing, S.A., Robison, T., Rothfels, C.J., Sigel, E.M., Song, Y., Timilsena, P.R., Van de Peer, Y., Wang, H., Wilhelmsson, P.K.I., Wolf, P.G., Xu, X., Der, J.P., Schluepmann, H., Wong, G.K.-S., Pryer, K.M., 2018. Fern genomes elucidate land plant evolution and cyanobacterial symbioses. Nat. Plants 4, 460–472. https://doi.org/10.1038/s41477-018-0188-8

Li, X., Fu, Q., Zhao, F.-X., Wu, Y.-Q., Zhang, T.-Y., Li, Z.-Q., He, J.-M., 2022. GCR1 Positively Regulates UV-B- and Ethylene-Induced Stomatal Closure via Activating GPA1-Dependent ROS and NO Production. Int. J. Mol. Sci. 23, 5512. https://doi.org/10.3390/ijms23105512

Li, Z., Guo, H., 2018. Ethylene Treatment in Studying Leaf Senescence in Arabidopsis. Methods Mol. Biol. Clifton NJ 1744, 105–112. https://doi.org/10.1007/978-1-4939-7672-0_8

Maillard, P., Thepenier, C., Gudin, C., 1993. Determination of an ethylene biosynthesis pathway in the unicellular green alga,Haematococcus pluvialis. Relationship between growth and ethylene production. J. Appl. Phycol. 5, 93–98. https://doi.org/10.1007/BF02182426

Mao, K., Zhang, M., Kong, Y., Dai, S., Wang, Y., Meng, Q., Ma, N., Lv, W., 2022. Origin, Expansion, and Divergence of ETHYLENE-INSENSITIVE 3 (EIN3)/EIN3-LIKE Transcription Factors During Streptophytes Evolution. Front. Plant Sci. 13. https://doi.org/10.3389/fpls.2022.858477

Meindl, T., Boller, T., Felix, G., 2000. The Bacterial Elicitor Flagellin Activates Its Receptor in Tomato Cells According to the Address–Message Concept. Plant Cell 12, 1783–1794. https://doi.org/10.1105/tpc.12.9.1783

Mirdita, M., Schütze, K., Moriwaki, Y., Heo, L., Ovchinnikov, S., Steinegger, M., 2022. ColabFold: making protein folding accessible to all. Nat Methods 19, 679–682. https://doi.org/10.1038/s41592-022-01488-1

Mou, Z., Eakes, J., Cooper, C.J., Foster, C.M., Standaert, R.F., Podar, M., Doktycz, M.J., Parks, J.M., 2021. Machine learning-based prediction of enzyme substrate scope: Application to bacterial nitrilases. Proteins Struct. Funct. Bioinforma. 89, 336–347. https://doi.org/10.1002/prot.26019

Nazli, Z.-H., Arshad, M., Khalid, A., 2003. 2-Keto-4-methylthiobutyric acid-dependent biosynthesis of ethylene in soil. Biol. Fertil. Soils 37, 130–135. https://doi.org/10.1007/s00374-002-0578-x

North, J.A., Narrowe, A.B., Xiong, W., Byerly, K.M., Zhao, G., Young, S.J., Murali, S., Wildenthal, J.A., Cannon, W.R., Wrighton, K.C., Hettich, R.L., Tabita, F.R., 2020. A nitrogenase-like enzyme system catalyzes methionine, ethylene, and methane biogenesis. Science 369, 1094–1098. https://doi.org/10.1126/science.abb6310

Park, H.L., Seo, D.H., Lee, H.Y., Bakshi, A., Park, C., Chien, Y.-C., Kieber, J.J., Binder, B.M., Yoon, G.M., 2023. Ethylene-triggered subcellular trafficking of CTR1 enhances the response to ethylene gas. Nat. Commun. 14, 365. https://doi.org/10.1038/s41467-023-35975-6

Patro, R., Duggal, G., Love, M.I., Irizarry, R.A., Kingsford, C., 2017. Salmon provides fast and bias-aware quantification of transcript expression. Nat. Methods 14, 417–419. https://doi.org/10.1038/nmeth.4197

Pattyn, J., Vaughan-Hirsch, J., Van de Poel, B., 2021. The regulation of ethylene biosynthesis: a complex multilevel control circuitry. New Phytol. 229, 770–782. https://doi.org/10.1111/nph.16873

Paysan-Lafosse, T., Blum, M., Chuguransky, S., Grego, T., Pinto, B.L., Salazar, G.A., Bileschi, M.L., Bork, P., Bridge, A., Colwell, L., Gough, J., Haft, D.H., Letunić, I., Marchler-Bauer, A., Mi, H., Natale, D.A., Orengo, C.A., Pandurangan, A.P., Rivoire, C., Sigrist, C.J.A., Sillitoe, I., Thanki, N., Thomas, P.D., Tosatto, S.C.E., Wu, C.H., Bateman, A., 2023. InterPro in 2022. Nucleic Acids Res. 51, D418–D427. https://doi.org/10.1093/nar/gkac993

Price, D.C., Chan, C.X., Yoon, H.S., Yang, E.C., Qiu, H., Weber, A.P.M., Schwacke, R., Gross, J., Blouin, N.A., Lane, C., Reyes-Prieto, A., Durnford, D.G., Neilson, J.A.D., Lang, B.F., Burger, G., Steiner, J.M., Löffelhardt, W., Meuser, J.E., Posewitz, M.C., Ball, S., Arias, M.C., Henrissat, B., Coutinho, P.M., Rensing, S.A., Symeonidi, A., Doddapaneni, H., Green, B.R., Rajah, V.D., Boore, J., Bhattacharya, D., 2012. *Cyanophora paradoxa* Genome Elucidates Origin of Photosynthesis in Algae and Plants. Science 335, 843–847. https://doi.org/10.1126/science.1213561

Price, D.C., Goodenough, U.W., Roth, R., Lee, J.-H., Kariyawasam, T., Mutwil, M., Ferrari, C., Facchinelli, F., Ball, S.G., Cenci, U., Chan, C.X., Wagner, N.E., Yoon, H.S., Weber, A.P.M., Bhattacharya, D., 2019. Analysis of an improved Cyanophora paradoxa genome assembly. DNA Res. 26, 287–299. https://doi.org/10.1093/dnares/dsz009

Price, D.C., Steiner, J.M., Yoon, H.S., Bhattacharya, D., Löffelhardt, W., 2016. Glaucophyta, in: Archibald, J.M., Simpson, A.G.B., Slamovits, C.H., Margulis, L., Melkonian, M., Chapman, D.J., Corliss, J.O. (Eds.), Handbook of the Protists. Springer International Publishing, Cham, pp. 1–65. https://doi.org/10.1007/978-3-319-32669-6_42-1

Qi, F., Zhang, F., 2020. Cell Cycle Regulation in the Plant Response to Stress. Front. Plant Sci. 10. https://doi.org/10.3389/fpls.2019.01765

R Core Team, 2013. R: A language and environment for statistical computing.

Schaller, A., Stintzi, A., Graff, L., 2012. Subtilases - versatile tools for protein turnover, plant development, and interactions with the environment. Physiol. Plant. 145, 52–66. https://doi.org/10.1111/j.1399-3054.2011.01529.x

Schaller, G.E., Kieber, J.J., 2002. Ethylene. Arab. Book 2002. https://doi.org/10.1199/tab.0071

Schieber, M., Chandel, N.S., 2014. ROS function in redox signaling and oxidative stress. Curr. Biol. CB 24, R453-462. https://doi.org/10.1016/j.cub.2014.03.034

Sehnal, D., Bittrich, S., Deshpande, M., Svobodová, R., Berka, K., Bazgier, V., Velankar, S., Burley, S.K., Koča, J., Rose, A.S., 2021. Mol* Viewer: modern web app for 3D visualization and analysis of large biomolecular structures. Nucleic Acids Res 49, W431–W437. https://doi.org/10.1093/nar/gkab314

Soneson, C., Love, M.I., Robinson, M.D., 2015. Differential analyses for RNA-seq: transcript-level estimates improve gene-level inferences. F1000Research 4, 1521. https://doi.org/10.12688/f1000research.7563.2

Sun, S., Gresham, D., 2021. Cellular Quiescence in Budding Yeast. Yeast Chichester Engl. 38, 12–29. https://doi.org/10.1002/yea.3545

Sun, Y., Pri-Tal, O., Michaeli, D., Mosquna, A., 2020. Evolution of Abscisic Acid Signaling Module and Its Perception. Front. Plant Sci. 11, 934. https://doi.org/10.3389/fpls.2020.00934

Tao, J.-J., Chen, H.-W., Ma, B., Zhang, W.-K., Chen, S.-Y., Zhang, J.-S., 2015. The Role of Ethylene in Plants Under Salinity Stress. Front. Plant Sci. 6. https://doi.org/10.3389/fpls.2015.01059

Thomma, B.P.H.J., Eggermont, K., Tierens, K.F.M.-J., Broekaert, W.F., 1999. Requirement of Functional Ethylene-Insensitive 2 Gene for Efficient Resistance of Arabidopsis to Infection by Botrytis cinerea. Plant Physiol. 121, 1093–1101. https://doi.org/10.1104/pp.121.4.1093

Tsavkelova, E.A., Klimova, S.Yu., Cherdyntseva, T.A., Netrusov, A.I., 2006. Hormones and hormone-like substances of microorganisms: A review. Appl. Biochem. Microbiol. 42, 229–235. https://doi.org/10.1134/S000368380603001X

Van de Poel, B., Van Der Straeten, D., 2014. 1-aminocyclopropane-1-carboxylic acid (ACC) in plants: more than just the precursor of ethylene! Front. Plant Sci. 5. https://doi.org/ 10.3389/fpls.2014.00640

Vaseva, I.I., Qudeimat, E., Potuschak, T., Du, Y., Genschik, P., Vandenbussche, F., Van Der Straeten, D., 2018. The plant hormone ethylene restricts Arabidopsis growth via the epidermis. Proc. Natl. Acad. Sci. 115, E4130–E4139. https://doi.org/10.1073/pnas.1717649115

Vij, S., Tyagi, A.K., 2008. A20/AN1 zinc-finger domain-containing proteins in plants and animals represent common elements in stress response. Funct. Integr. Genomics 8, 301–307. https://doi.org/10.1007/s10142-008-0078-7

von Dahl, C.C., Baldwin, I.T., 2007. Deciphering the Role of Ethylene in Plant–Herbivore Interactions. J. Plant Growth Regul. 26, 201–209. https://doi.org/10.1007/s00344-007-0014-4

Walter, W., Sánchez-Cabo, F., Ricote, M., 2015. GOplot: an R package for visually combining expression data with functional analysis. Bioinforma. Oxf. Engl. 31, 2912–2914. https://doi.org/10.1093/bioinformatics/btv300

Wei, S., Zhang, W., Fu, R., Zhang, Y., 2021. Genome-wide characterization of 2-oxoglutarate and Fe(II)-dependent dioxygenase family genes in tomato during growth cycle and their roles in metabolism. BMC Genomics 22, 126. https://doi.org/10.1186/s12864-021-07434-3

Yordanova, Z.P., Iakimova, E.T., Cristescu, S.M., Harren, F.J.M., Kapchina-Toteva, V.M., Woltering, E.J., 2010. Involvement of ethylene and nitric oxide in cell death in mastoparan-treated unicellular alga Chlamydomonas reinhardtii. Cell Biol. Int. 34, 301–308. https://doi.org/10.1042/CBI20090138

Zepernick, B.N., Niknejad, D.J., Stark, G.F., Truchon, A.R., Martin, R.M., Rossignol, K.L., Paerl, H.W., Wilhelm, S.W., 2022. Morphological, physiological, and transcriptional responses of the freshwater diatom Fragilaria crotonensis to elevated pH conditions. Front. Microbiol. 13, 1044464. https://doi.org/10.3389/fmicb.2022.1044464

Zhang, W., Wen, C.-K., 2010. Preparation of ethylene gas and comparison of ethylene responses induced by ethylene, ACC, and ethephon. Plant Physiol. Biochem. 48, 45–53. https://doi.org/10.1016/j.plaphy.2009.10.002

Zhang, X., Wang, D., Elberse, J., Qi, L., Shi, W., Peng, Y.-L., Schuurink, R.C., Van den Ackerveken, G., Liu, J., 2021. Structure-guided analysis of Arabidopsis JASMONATE-INDUCED OXYGENASE (JOX) 2 reveals key residues for recognition of jasmonic acid substrate by plant JOXs. Mol. Plant 14, 820–828. https://doi.org/10.1016/j.molp.2021.01.017

Zwiewka, M., Nodzyński, T., Robert, S., Vanneste, S., Friml, J., 2015. Osmotic Stress Modulates the Balance between Exocytosis and Clathrin-Mediated Endocytosis in Arabidopsis thaliana. Mol. Plant 8, 1175–1187. https://doi.org/10.1016/j.molp.2015.03.007

FIGURE 1

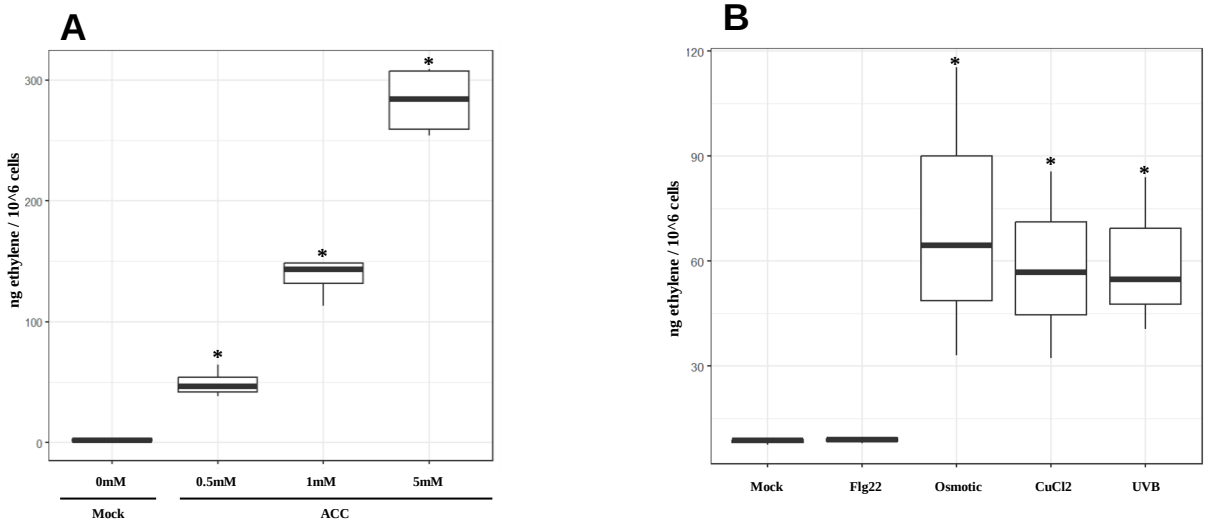

FIGURE 2

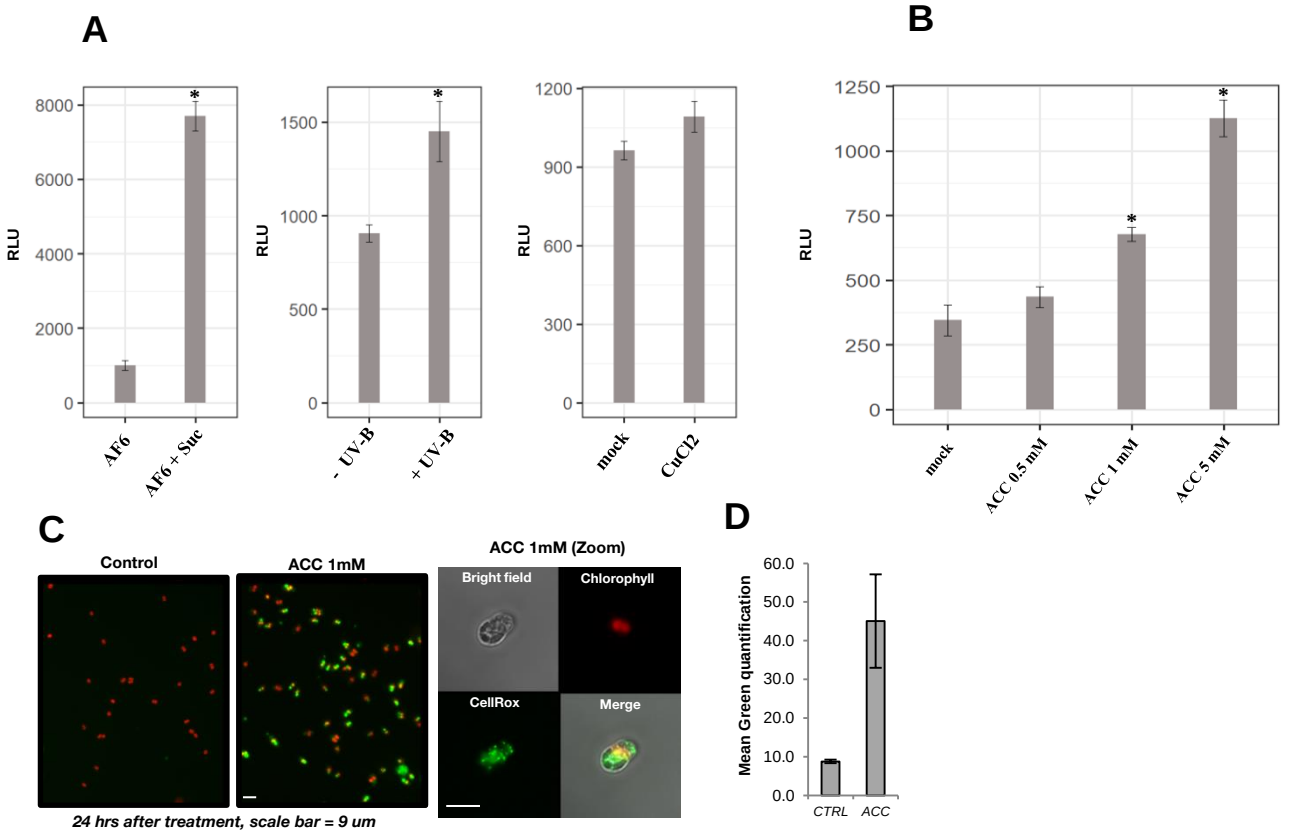

FIGURE 3

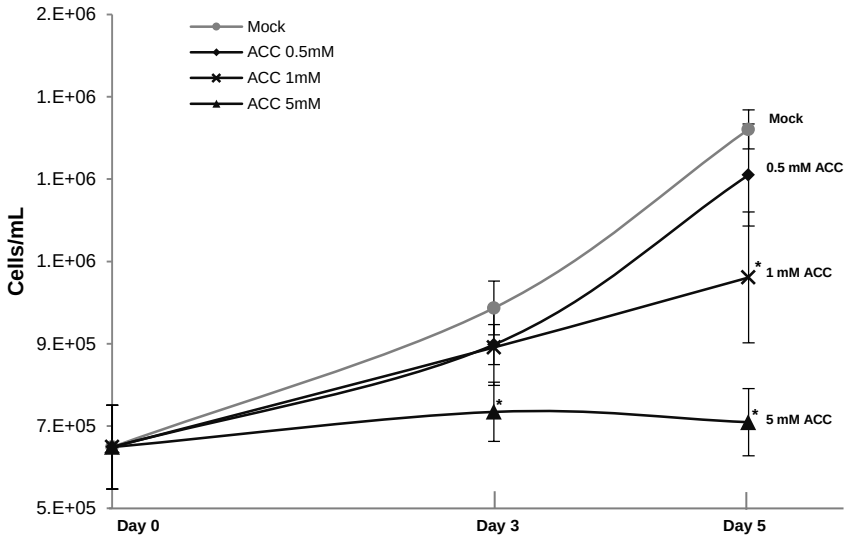

FIGURE 4

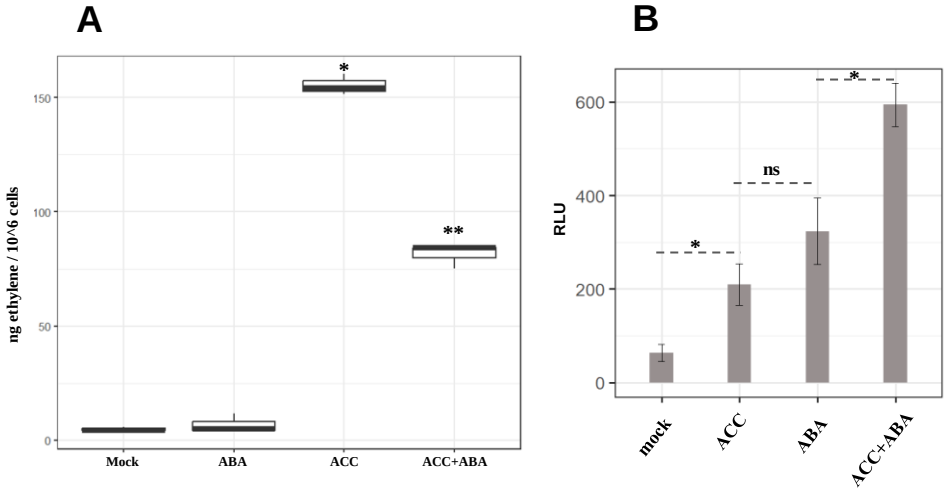

FIGURE 5

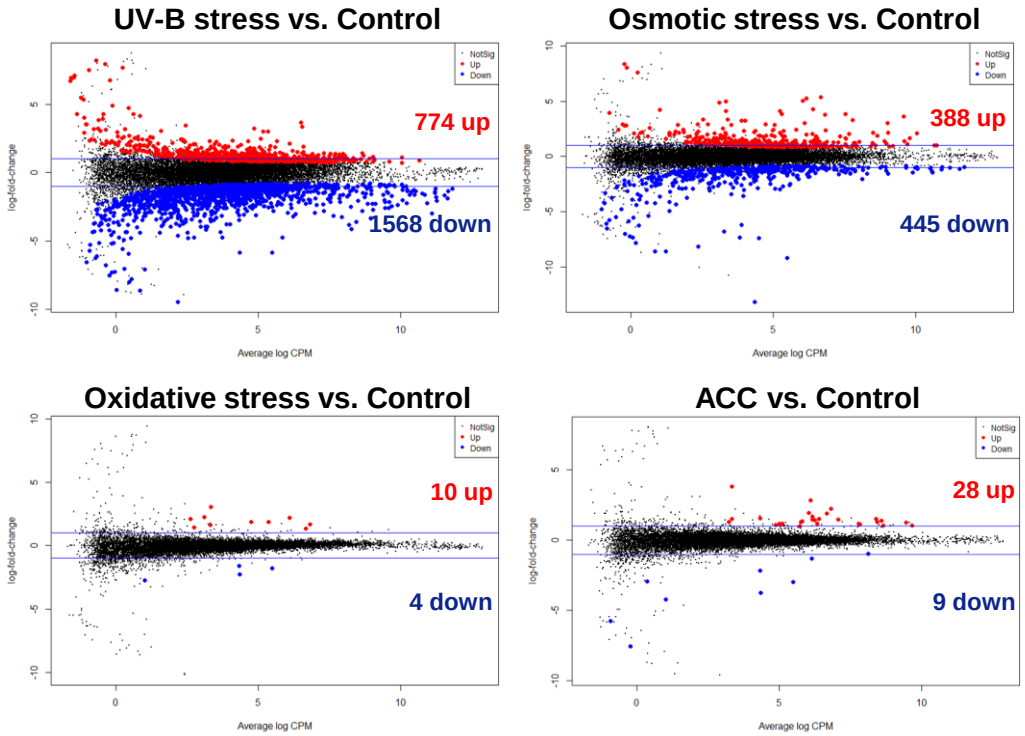

FIGURE 6

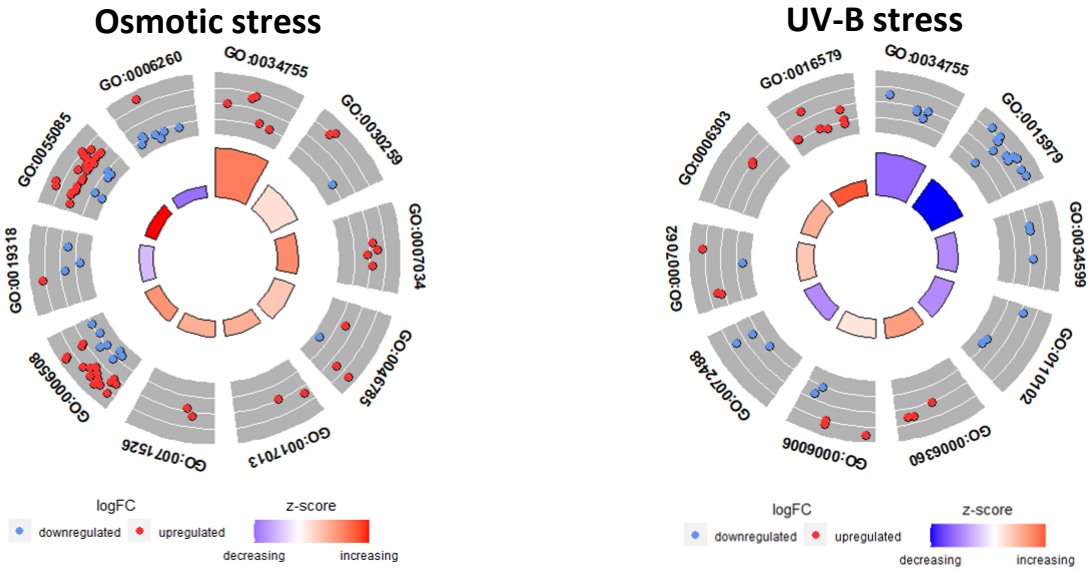

Osmotic stress

ID	Description
GO:0034755	iron ion transmembrane transport
GO:0030259	lipid glycosylation
GO:0007034	vacuolar transport
GO:0046785	microtubule polymerization
GO:0017013	protein flavinylation
GO:0071526	semaphorin-plexin signaling pathway
GO:0006508	proteolysis
GO:0019318	hexose metabolic process
GO:0055085	transmembrane transport
GO:0006260	DNA replication

UV-B

ID	Description
GO:0034755	iron ion transmembrane transport
GO:0015979	photosynthesis
GO:0034599	cellular response to oxidative stress
GO:0110102	ribulose bisphosphate carboxylase complex assembly
GO:0006360	transcription by RNA polymerase I
GO:0006006	glucose metabolic process
GO:0072488	ammonium transmembrane transport
GO:0007062	sister chromatid cohesion
GO:0006303	double-strand break repair via nonhomologous end joining
GO:0016579	protein deubiquitination

ACC

ID	Description
GO:0006508	proteolysis
GO:0006388	tRNA splicing, via endonucleolytic cleavage and ligation
GO:0046785	microtubule polymerization

Oxidative stress

ID	Description
GO:0046785	microtubule polymerization
GO:0006508	proteolysis

FIGURE 7

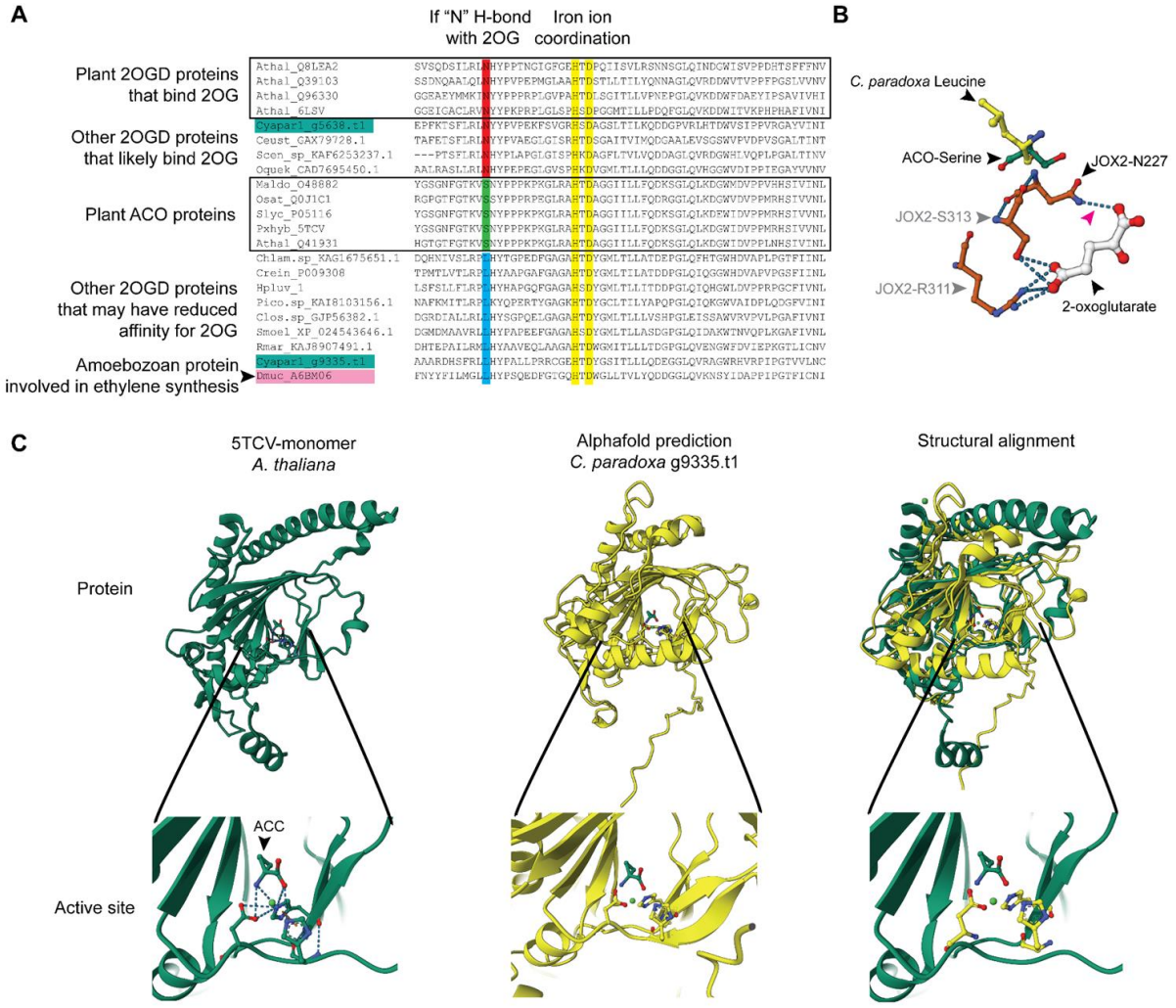
A
If "N" H-bond with 2OG
Iron ion coordination
Plant 2OGD proteins that bind 2OG
Athal_Q8LEA2
Athal_Q39103
Athal_Q96330
Athal_6LSV
Other 2OGD proteins that likely bind 2OG
Cyapa1_g9638.t1
Ceust_GAX79728.1
Scen_sp_KAF6253237.1
Oquek_CAD7695450.1
Plant ACO proteins
Maldo_O48882
Osat_Q0J1C1
Slyc_P05116
Pxhyb_5TCV
Athal_Q41931
Other 2OGD proteins that may have reduced affinity for 2OG
Chlam.sp_KAG1675651.1
Crein_P009308
Hpluv_1
Pico.sp_KAI8103156.1
Clos.sp_GJP56382.1
Smoel_XP_024543646.1
Rmar_KAJ8907491.1
Cyapa1_g9335.t1
Amoebozoan protein involved in ethylene synthesis
Dmuc_A6BM06
B
C. paradoxa Leucine
ACO-Serine
JOX2-N227
JOX2-S313
JOX2-R311
2-oxoglutarate
C
5TCV-monomer
A. thaliana
Alphafold prediction
C. paradoxa g9335.t1
Structural alignment
Protein
Active site
ACC

FIGURE 8

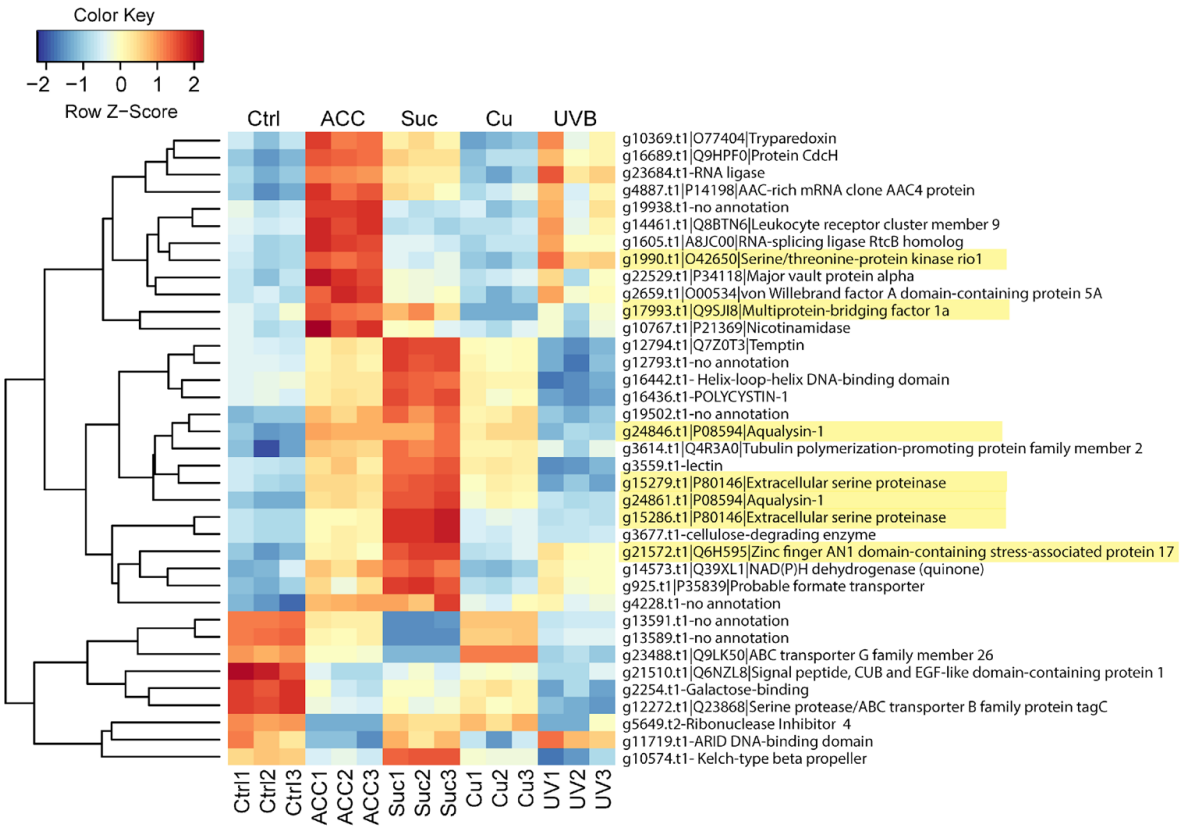

FIGURE 9

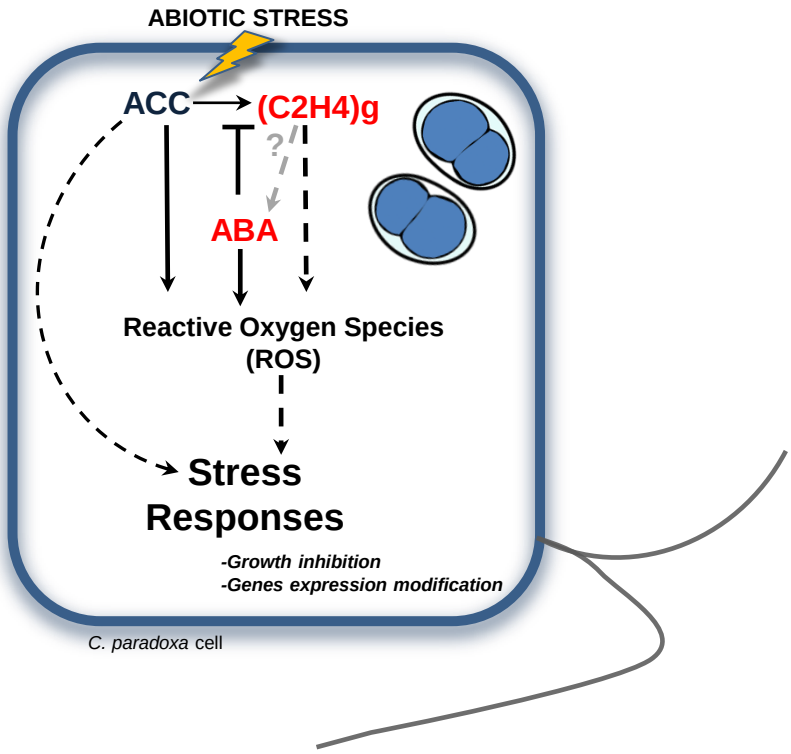

Suppl.Fig1

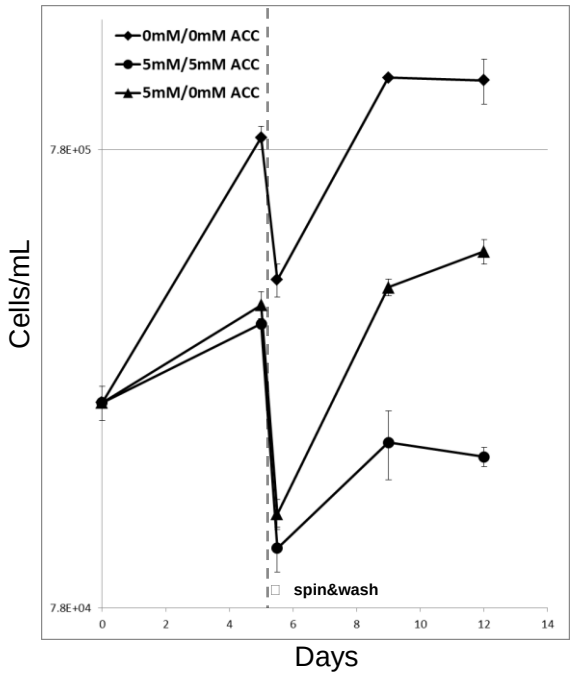

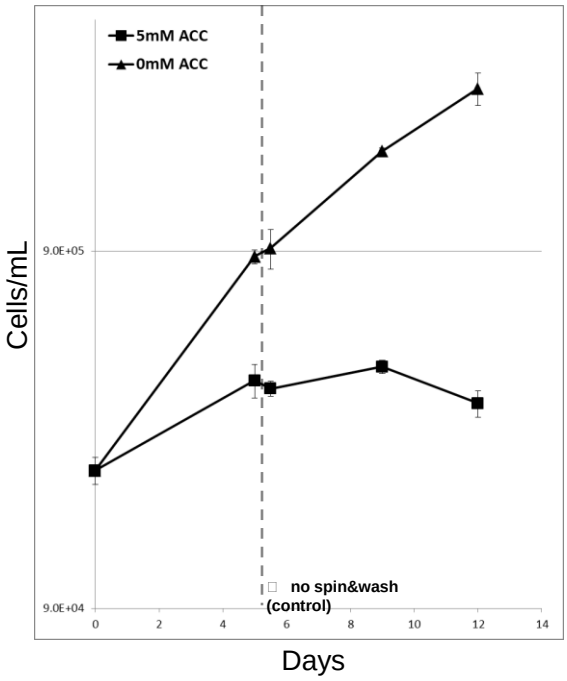

Day 12 pictures

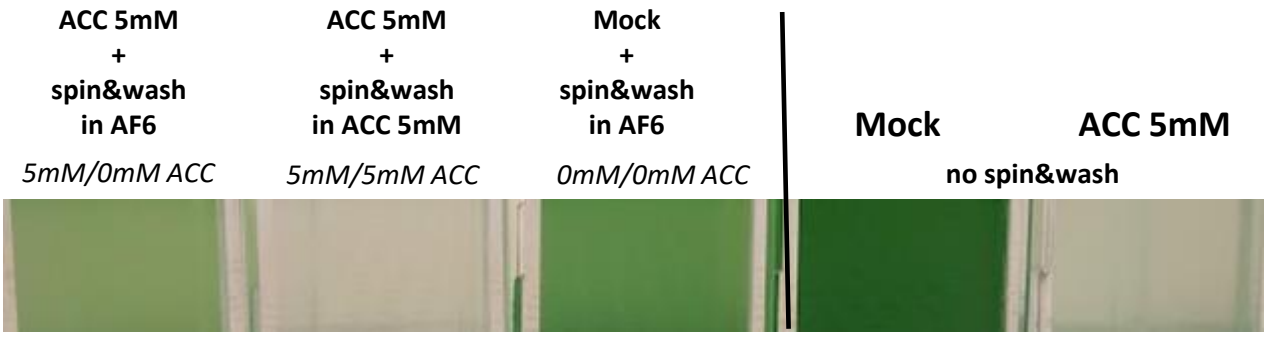

Suppl Fig1 : ACC-dependent growth inhibition is relieved after washing off ACC from the media.

C.paradoxa cell concentrations over 12 days after 5 mM ACC or mock treatments. For each time point, cell concentrations were monitored on day 0, day 5, day 9 and day 12 using a hemocytometer. 20 mL cultures of *C.paradoxa* were treated with 5 mM ACC or mock (water) and incubated in a culture chamber for 5 days. Left panel : At day 5, cells were spin and washed two times in AF6 media before being replaced in 20mL vial and treated with ACC or mock, creating three distinct conditions : ACC + spin/wash in ACC (circle) ; ACC + spin/wash in mock (triangle) ; mock + spin/wash in mock (diamond). Right panel : At day 5, cells were not washed and growth was monitored at day 9 and 12. 5 mM ACC treatment (square), mock treatment (triangle). Pictures (bottom): Representatives cultures used for this experiment at day 12 (final point).

Suppl.Fig2

A Cyclin expression across samples

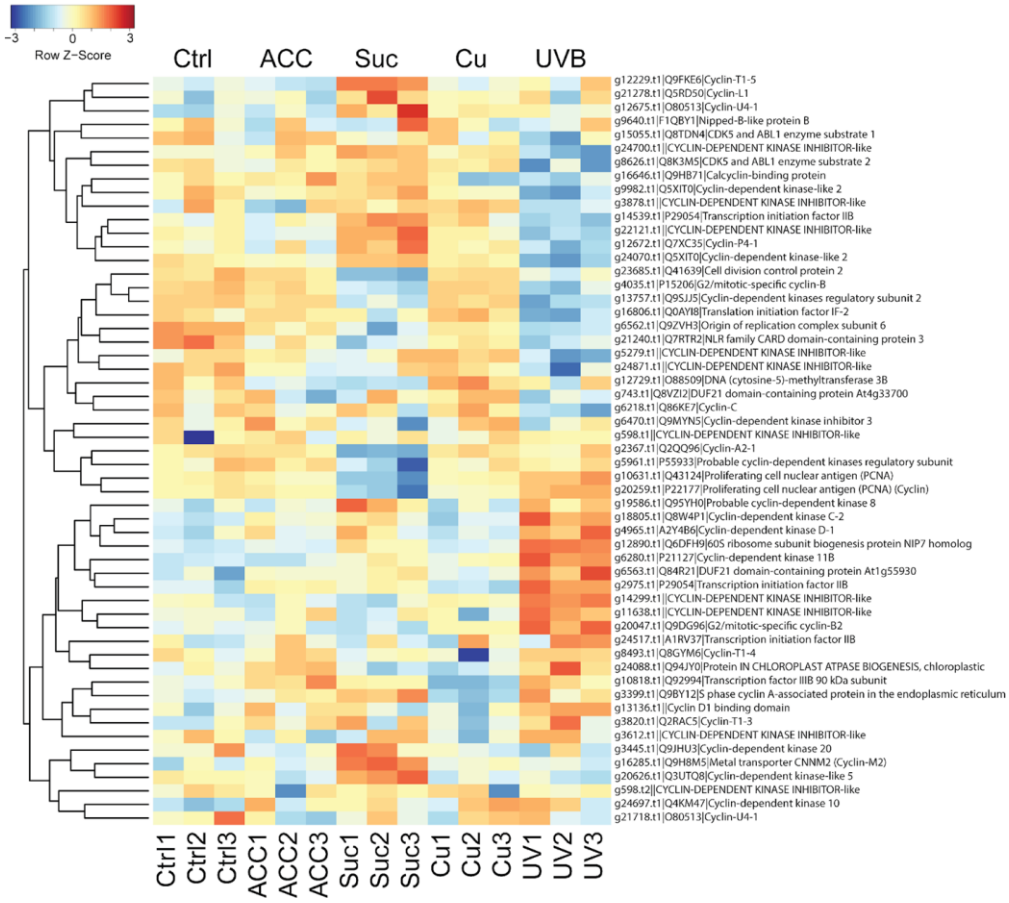
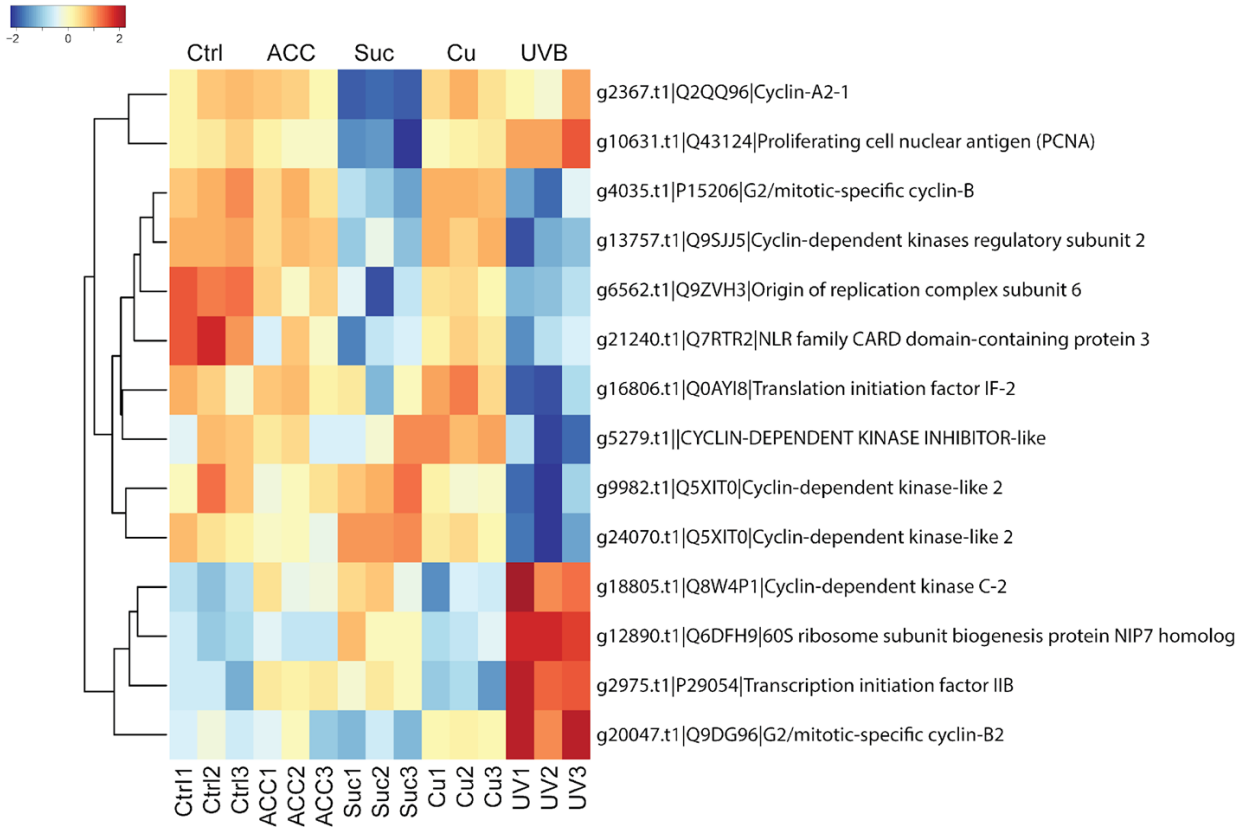
B Differentially expressed cyclins and CDKs